RSC Advances

PAPER

View Article Online
View Journal | View Issue

Cite this: *RSC Adv.*, 2026, **16**, 13821

Ultra-fast capture of U(VI) from aqueous solutions by chitosan-based foam with macropores

Lirong Yang,[a] Tingdong Zhou,[b] Yuqian Jiang,[a] Huizhou Chen,[a] Wenjing Yang,[a] Haoyu Huang,[a] Jianguo Gao,[c] Deming Huang*[d] and Jie Tang *[a]

Received 20th June 2025
Accepted 26th January 2026

DOI: 10.1039/d5ra04402b

rsc.li/rsc-advances

The construction and preparation of macroporous materials with strong uranium coordination groups are conducive to fast uranium capture from aqueous solutions. Herein, a novel eco-friendly glutamine-functionalized chitosan foam (CS-Gln) with a three dimensional macroporous structure was prepared for ultra-fast uranium capture. The uranium adsorption amount is 23 mg g^{-1} within 2 min, which accounts for 92% of the equilibrium adsorption amount; equilibrium adsorption can be reached within 30 min, with an adsorption amount of 25 mg g^{-1}. Moreover, the uranium adsorption process is more consistent with pseudo-second-order kinetics and the Sips isothermal model, with a maximum uranium sorption amount of 294 mg g^{-1}. Uranium adsorption involves both electrostatic and coordination interactions. The coordination adsorption is dominant, with −COOH, $-NH_2$ and −C═N as the main coordination groups. The experiments provide effective insights into the preparation of an ultrafast chitosan-based uranium adsorbent.

1 Introduction

Nuclear energy, the fourth largest power generation source after thermal energy, hydroelectric power, and renewable energy, is one of the main sources of clean energy all over the world.[1] Currently, nuclear energy, accounting for about 25% of the global electricity generation, has the potential to reduce CO_2 emissions by about 1 gigatonne per year.[2] Due to its low carbon emissions, the scale of global nuclear power generation has been increasing. Uranium is one of the main elements for nuclear power generation, but the current uranium reserves can only meet the supply for 90 years.[3] Additionally, uranium-containing wastewater can seriously damage the ecological environment. In addition to the nuclear waste pollution caused by improper uranium waste disposal, the three famous nuclear leakage incidents in history (the Three Mile Island Accident in 1979,[4] the Chernobyl nuclear accident in 1986,[5] and the Fukushima Daiichi NPS accident in 2011 (ref. 6)) have caused large-scale nuclear waste pollution and will have a great lasting influence on human physical and mental health in the future.[7] Therefore, the recovery and disposal of uranium are particularly important for environmental protection.

Thus far, among the developed uranium recovery and disposal technologies, such as adsorption[8] and photoreduction,[9,10] adsorption has become one of the most promising technologies for uranium capture due to its easy operation, high efficiency and good recoverability.[11] The development of high-performance adsorbents is a crucial aspect of adsorption technology. Compared with inorganic materials, such as Al_2O_3,[12] SiO_2 (ref. 13) and TiO_2,[14] polymer materials are more welcomed because of their strong coordination groups with uranium. Chitosan, the second most abundant natural polymer, is a pseudo-natural polysaccharide extracted from chitin. It has gradually become the focus of research owing to its rich reserves, non-toxicity, and abundant surface functional groups.[15] The capture amount of uranium for pure chitosan can reach 483 mg g^{-1}.[16] However, the intramolecular/intermolecular interaction of chitosan prevents the rapid approach of uranyl ions to the active sites, resulting in a longer equilibrium uptake time of up to 5 h.[16,17] It has been reported that cross-linking can increase the rate of adsorption of chitosan for uranium.[16] For example, Qi Ren[18] prepared CTS membranes by crosslinking chitosan with glutaraldehyde, whose adsorption equilibrium time for uranium was shortened to 45 min. However, the uranium adsorption capacity of CTS decreased to 26 mg g^{-1} because the active amino groups on the chitosan chain were occupied after crosslinking. Therefore, in order to shorten the equilibrium adsorption time while maintaining the adsorption capacity, various efforts have been made to improve the adsorption amount of the crosslinked chitosan by introducing strong ligand uranium groups containing N/O. For example, Qi Ren

[a]School of Chemistry and Chemical Engineering, Mianyang Teachers' College, Mianyang 621000, PR China
[b]Key Laboratory of Materials and Surface Technology (Ministry of Education), School of Materials Science and Engineering, Xihua University, Chengdu, 610039, PR China
[c]School of Foreign Languages, Mianyang Teachers' College, Mianyang 621000, PR China
[d]School of Mechanical and Electrical, Mianyang Teachers' College, Mianyang 621000, PR China

et al.[18] prepared PEI/CS by introducing polyethyleneimine to chitosan, which contains abundant amino groups. The capture amount of PEI/CS for uranium is 291 mg g^{-1}, but its equilibrium time is 3 h, which is four times longer than that of pure chitosan. Therefore, it is of great scientific significance to design chitosan-based adsorbents for the rapid adsorption of U(VI).

It is generally believed that hierarchical porous materials with macropores, mesopores and micropores can improve the adsorption rate by enhancing the transport of metal ions and promoting their effective reaction with the active sites in the material.[19–21] However, the presence of a large amount of micropores and mesopores may cause the entrapment of uranyl ions within the pores, which reduces the adsorption rate.[22,23] From this point of view, if chitosan is prepared as a porous material dominated by macropores, the equilibrium adsorption time may be shortened by promoting the flow of uranyl ions. Many studies have proven that sol–gel can be used to prepare hydrogels composed of a three-dimensional elastic network with liquids in the gap space.[24,25] Freeze-drying can maintain the three-dimensional structure of the hydrogel without collapsing, and the dominant pores in the material are macropores.[26]

Therefore, a cross-linked chitosan hydrogel was prepared using the sol–gel method. Meanwhile, the eco-friendly glutamine (Gln) with abundant –COOH and $–NH_2$, which has a strong coordination ability with uranium, was introduced into chitosan to maintain the active sites of the material.[27] Furthermore, the chitosan-based foam (CS-Gln) dominated by macropores was successfully prepared by freeze-drying the hydrogel. The adsorption properties and adsorption mechanisms of CS-Gln for uranium were further studied.

2 Materials and methods

2.1 Materials

Chitosan (CS, degree of deacetylation > 95%), glutamine (Gln), *p*-phthalaldehyde (PTA), uranyl nitrate hexahydrate ($UO_2(NO_3)_2 \cdot 6H_2O$), arson azo III, dimethyl sulfoxide (DMSO), sodium hydroxide (NaOH), hydrochloric acid (HCl), 1,4-dioxane and glacial acetic acid are all analytically pure and were not further purified before use.

2.2 Preparation of CS-Glns

As shown in Fig. 1, CS-Glns were prepared as follows. 0.5 g CS and 0.75 g Gln were dissolved in 30 mL (2%, v/v) glacial acetic acid and stirred until a clear and transparent solution was obtained (solution A). 0.4 g of PTA was dissolved in 10 mL1, 4-dioxane (solution B). Afterward, solution B was slowly added into solution A and stirred. Well mixed, the mixture solution was left undisturbed at 60 °C for 16 h to form a hydrogel. Finally, the sample was washed several times with 1, 4-dioxane and freeze-dried. A yellow porous CS-Gln1 foam was successfully achieved. Additionally, when the weight of Gln was adjusted to 0.5 g and 0.25 g, the obtained samples were denoted by CS-Gln2 and CS-Gln3, respectively.

2.3 Characterization

The surface functional groups of the CS-Glns were tested using a Fourier transform infrared spectrometer (FT-IR, Thermo Scientific, USA). Energy-dispersive X-ray with scanning electron microscopy (SEM-EDX, Thermo Scientific, USA) was used to observe the micro-morphology and elemental distribution of the materials. N_2 adsorption/desorption isothermal curves were obtained using a Quantachrome Autosorb NOVA2200e (USA).

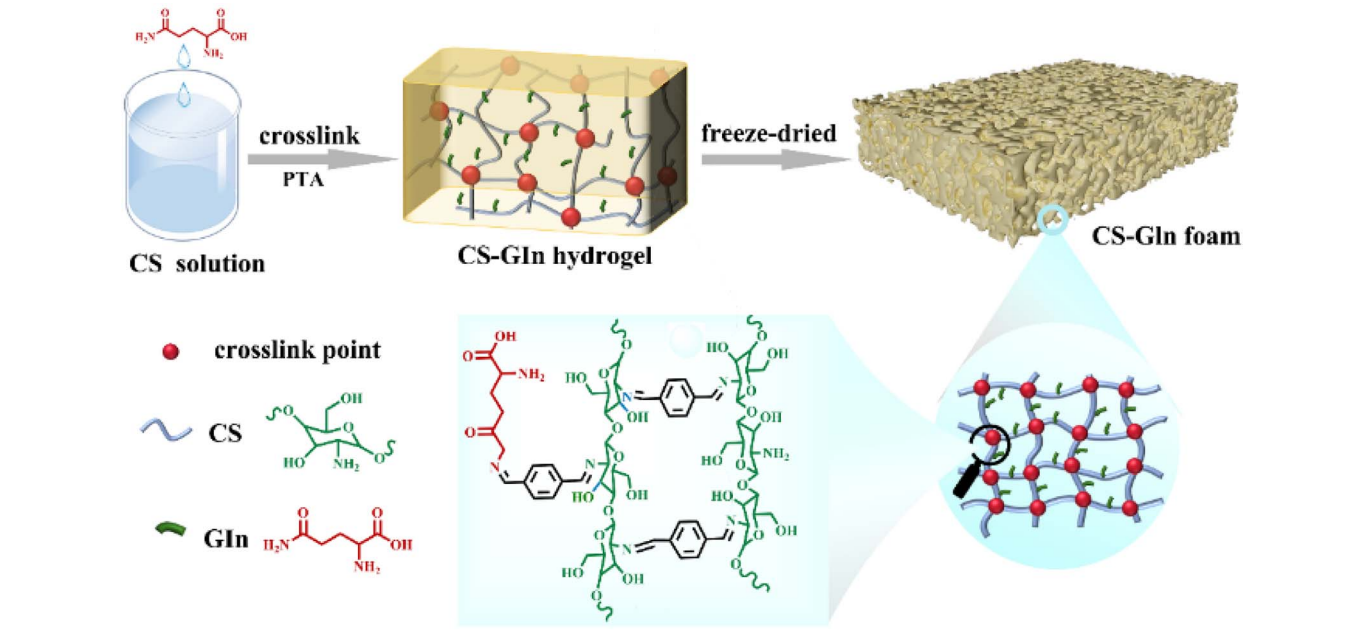

Fig. 1 Schematic of the preparation of CS-Gln.

The surface areas and pore size distribution were fitted using BJH. The chemical properties and compositions of the material surfaces were tested using X-ray photoelectron spectroscopy (XPS, Thermo Scientific, USA). The surface charge of the material at different pH values was detected using a Malvern Zetasizer Nano ZS90 (USA), and the isoelectric point was determined. The pH value of the solutions was monitored using a pH meter (Inesa Scientific, China).

2.4 Batch adsorption experiments

In order to study the uranium sorption properties of CS-Glns, the relationship between pH value, contact time, initial uranium concentration and sorption amount was studied. The ratio between the volume of the uranium solution at various concentrations and the weight of the adsorbent is about 10 : 1. The pH value of the solution is regulated by 0.1 mol L^{-1} HCl or NaOH. After a period of thermostatic agitation, the supernatant was filtered, and its concentration was detected by applying the arsenazo III-based spectrophotometric method. To minimize errors, all experiments were repeated three times, and the average value was taken as the final adsorption amount. The adsorption amount (q_e) was calculated using the following formula:

$$q_e = \frac{(C_0 - C_e) \times V}{m},$$

where q_e is the adsorption amount. C_0 and C_e represent the UO_2^{2+} concentrations before and after capture, respectively. V and m are the volume of the UO_2^{2+} solution and the weight of CS-Gln, respectively.

3 Results and discussion

3.1 Structural and morphological characterization

The functional groups of CS and CS-Glns were identified using FT-IR (Fig. 2). For pure chitosan (CS), the broadening peak of the overlapping –OH and –NH stretching vibrations is located at 3435 cm^{-1}. Additionally, there are stretching vibrations of C–H on the CS skeleton at 2971 cm^{-1}, C–O at 1384 cm^{-1}, C–O–C at 1152 cm^{-1}, amide I at 1647 cm^{-1}, amide II band at 1601 cm^{-1} and β-glycosidic at 897 cm^{-1}. At the same time, the stretching vibration peak of C–O from C_3–OH is observed at 1090 cm^{-1}. These results are consistent with those of previous reports.[28–30] After reacting with Gln, the three spectra show a high degree of similarity, with new peaks appearing. The peak at 1641 cm^{-1} corresponds to C=N, while the peak at 1691 cm^{-1} corresponds to the overlapping of –COOH and –CHO. Besides, all peaks at 1573 cm^{-1}, 1488 cm^{-1} and 1450 cm^{-1} are benzene ring skeleton vibration peaks. These results indicate that CS and Gln are successfully cross-linked and that CS-Gln is synthesized. The potential reaction mechanism is illustrated in Fig. S1.

SEM images of CS-Glns are illustrated in Fig. 3. There are obvious macropores with high pore size connectivity in the three samples. Among them, CS-Gln2 has the largest porosity and the best pore flow. The N_2 adsorption–desorption isotherms and pore size distribution are displayed in Fig. 4. Due to the lack of mesopores and micropores, the specific surface areas of the CS-Glns are rather low (Table 1), which are 24.529 $m^2\ g^{-1}$, 20.471 $m^2\ g^{-1}$ and 9.748 $m^2\ g^{-1}$. In a relatively high pressure (P/P_0) range, the N_2 adsorption–desorption isotherms of CS-Glns show very small hysteresis loops, and only a tiny condensation part is observed in the absorption branch. This tiny hysteresis is mainly caused by the absence of mesoporous.[31] Meanwhile, the peaks of the pore size distribution are diverse, while the intensities of both the micropores and mesopores is rather low. Additionally, the pore volumes of CS-Glns are only 0.025 $cm^3\ g^{-1}$, 0.023 $cm^3\ g^{-1}$ and 0.013 $cm^3\ g^{-1}$. These results show that the adsorbent is mainly composed of macropores, with a very small amount of mesopores and micropores. The structure dominated by macropores is conducive to promoting the flow and capture of uranyl ions on the surface of the

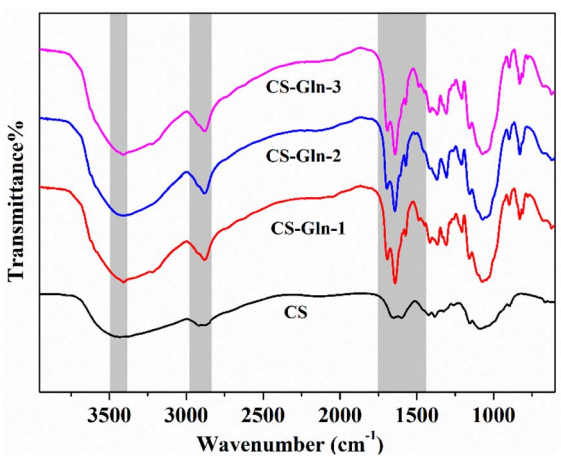

Fig. 2 FT-IR spectra of CS and CS-Glns.

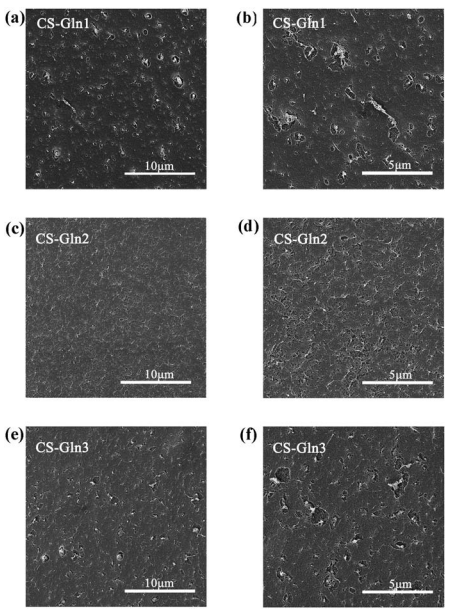

Fig. 3 SEM images of (a) and (b) CS-Gln1, (c) and (d) CS-Gln2, and (e) and (f) CS-Gln3.

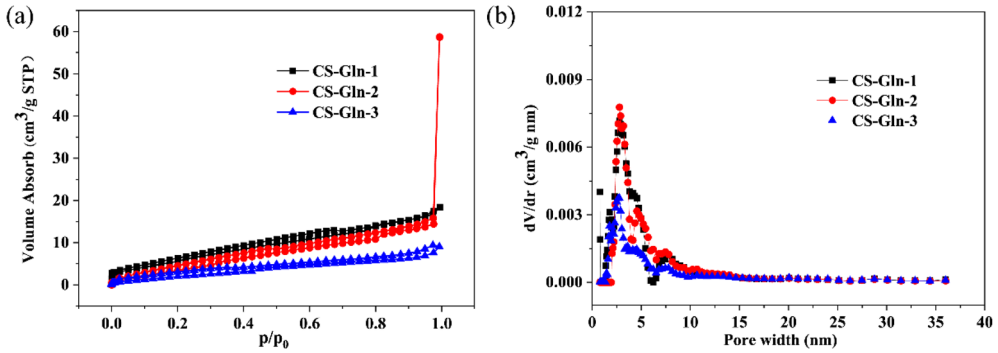

Fig. 4 (a) N_2 adsorption–desorption isotherms and (b) pore size distribution of CS-Glns.

Table 1 Specific surface areas and pore volume of CS-Glns

Sample	BET ($m^2\ g^{-1}$)	Total pore volume ($cm^3\ g^{-1}$)
CS-Gln1	24.529	0.025
CS-Gln2	20.471	0.023
CS-Gln3	9.748	0.013

samples. Thus, the sorption rate increases.[22] In addition, the ratio of CS and Gln in CS-Gln-2 is comparatively appropriate, while Gln in CS-Gln-1 and CS-Gln-3 is too much or too little, considering the reaction ratio and reaction mechanism (Table S1). Therefore, the proportion of amino or carboxyl groups in the material decreases, which results in the reduction of the uranium adsorption capacity. It can be inferred that the uranium adsorption capacity of CS-Gln2 is maximum.

3.2 Adsorption uranium

3.2.1 Effect of pH. When pH is less than 4, uranium is mainly in the form of UO_2^{2+}; when pH is in the range of 4–7, the polynuclear hydroxide $(UO_2)_n(OH)^{m+}$ becomes gradually dominant; and when pH is greater than 7, $(UO_2)_n(OH)^{m-}$ starts to appear in the solution and its proportion gradually increases with increasing pH.[17,18]

Meanwhile, the surface charge of CS-Glns is related to the pH value of the solution (Fig. 5a). When pH < pH_{IEP}, the surface charge of CS-Glns is positive; when pH > pH_{IEP}, it is negative. As depicted in Fig. 5a, the isoelectric points of CS-Gln1, CS-Gln2 and CS-Gln3 are 5.59, 6.49 and 4.53, respectively. The uranium adsorption of CS-Glns was investigated when 4 < pH < 10 (Fig. 5b). The trend of uranium adsorption capacity of the three samples at different pH values is basically the same.

When 4 < pH < pH_{IEP}, with an increase in pH, the coordination between gradually deprotonated $-NH_2$, –OH and –COOH

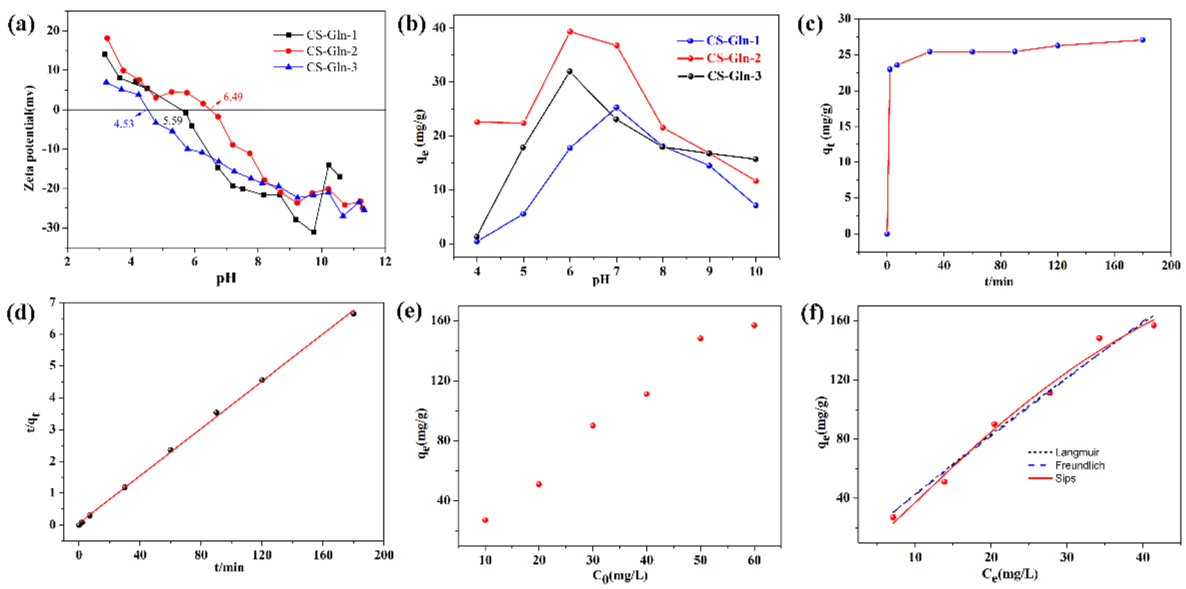

Fig. 5 (a) Zeta potential of CS-Glns, (b) effect of pH on the sorption amount ($m_{sorbent}/V_{solution}$ = 0.1 mg mL^{-1}, $[U]_{initial}$ = 10 mg L^{-1}, T = 298 K, contact time: 24 h), (c) relationship between the contact time and sorption amount ($m_{sorbent}/V_{solution}$ = 0.1 mg mL^{-1}, $[U]_{intial}$ = 10 mg L^{-1}, T = 298 K, pH = 6 ± 0.1), (d) line plots of pseudo-second-order model, (e) initial concentration of U(VI) and sorption amount ($m_{sorbent}/V_{solution}$ = 0.25 mg mL^{-1}, T = 298 K, pH = 6 ± 0.1) and (f) isothermal fitting curves.

groups with U(VI) is gradually enhanced as the pH increases, which improves the uranium adsorption capacity of CS-Gln.[32] However, there is electrostatic repulsion between the surface of positively charged CS-Glns and polynuclear hydroxide $(UO_2)_n(OH)^{m+}$. The surface positive charge of CS-Glns gradually decreases as the pH increases, thus leading to a gradual decrease in the electrostatic repulsion between CS-Glns and U(VI). With the effect of the above two factors, the uranium uptake amount of CS-Glns gradually increases. When pH increases from pH_{IEP} to 6, the surface charge of CS-Gln3 and CS-Gln2 becomes negative. Therefore, the interaction between the adsorbents and U(VI) changes from electrostatic repulsion to electrostatic attraction, leading to a further increase in uranium adsorption capacity as the pH increases. Among the three samples, CS-Gln3 has the lowest isoelectric point (pH 4.53). Therefore, when pH < 6, CS-Gln3 has the fastest capture rate for uranium and reaches its maximum sorption amount at pH 6, which is 31 mg g^{-1}. Meanwhile, CS-Gln2 reaches the maximum sorption amount for U(VI) at pH 6, which is 39 mg g^{-1}. When 7 < pH < 6, the gradual decrease in the surface negatively charged of CS-Gln1 leads to an increase in the electrostatic attraction between the material and the uranyl ion, resulting in a further increase in the uranium adsorption amount. The maximum sorption amount for U(VI) of CS-Gln1 reaches 25 mg g^{-1} at pH 7. At the same time, the surface charge of CS-Gln2 gradually changes from positive to negative in this pH range. Therefore, the uranium adsorption amount of CS-Gln2 decreases gradually. These results indicate that the effect of CS-Gln2 on uranyl ions is dominated by coordination. Additionally, both exhibit both electrostatic attraction and coordination between CS-Gln1, CS-Gln3 and uranium. When the pH is greater than 7, the surface charge decreases as the pH increases, leading to a gradual increase in the electrostatic repulsion between the adsorbents and the progressively dominant $(UO_2)_n(OH)^{m-}$. Therefore, the uranium adsorption amount of CS-Glns gradually decreases. Among the three samples, CS-Gln2 has the largest uranium sorption amount. This result coincides with the former inference.

3.2.2 Effect of contact time. The relationship between the uranium capture amount and contact time of CS-Gln2 at 10 mg L^{-1} and pH 5 was investigated (Fig. 5c). The basic sorption equilibrium can be reached within 2 min, and the sorption amount is 23 mg g^{-1}, which is 90% of the equilibrium sorption amount. The complete sorption equilibrium can be achieved within 30 min, with the sorption amount of 25.4 mg g^{-1}. The ultra-fast capture rate can be attributed to the three-dimensional channels and the presence of macropores in CS-Gln.[21] More specifically, this is because macropores can reduce the mass transfer diffusion resistance and promote adsorption, which improves the adsorption rate.[26,33,34]

In order to further investigate the sorption mechanism, the experimental data were fitted by the pseudo-first-order and pseudo-second-order kinetic models. The correlation linear fitting diagrams (Fig. S2 and 5d) and model parameters were obtained (Table 2). Compared with curves fitted by the pseudo-first-order kinetic, that of the pseudo-second order has a higher linearity, with a correlation coefficient (R^2) as high as 0.998. Moreover, the equilibrium capture amount fitted by pseudo-second-order kinetics is 26.8 mg g^{-1}, which is closer to the experimental data (25.4 mg g^{-1}). Therefore, it can be concluded that the experiment is more in accordance with the pseudo-second-order kinetic model, which is primarily influenced by chemisorption.[35]

3.2.3 Effect of solution concentration. The uranium sorption of CS-Gln2 was studied at 298 K with initial U(VI) concentrations from 10 mg L^{-1} to 60 mg L^{-1} (Fig. 5e). The uranium sorption amount gradually increases with an increase in the initial uranium concentration. When the initial concentration of U(VI) is 60 mg g^{-1}, the capture amount reaches up to 156 mg g^{-1}.

The experimental data were fitted by the Freundlich, Langmuir and Sips isothermal models (see the formulas in SI-3). The relevant fitting graph and model parameters were obtained (Fig. 5d, Tables 3 and S1). Adsorption takes place on a homogeneous monolayer according to the Langmuir isothermal model, with adsorption solely at specific sites and no interaction between them.[36] Additionally, the Freundlich isothermal model is generally appropriate for heterogeneous multilayer adsorption.[37] The Sips model combines the characteristics of the Langmuir and Freundlich models and considers the saturation and heterogeneity of the solution. More specifically, at low concentrations, it fits Freundlich's multilayer adsorption, while at high concentrations, it fits Langmuir's monolayer

Table 2 Kinetic parameters of pseudo-first-order and pseudo-second-order models

		Pseudo-first-order			Pseudo-second-order		
Sample	$q_{e,exp}$ (mg g^{-1})	$q_{e,cal}$ (mg g^{-1})	k_1 (min^{-1})	R^2	$q_{e,cal}$ (mg g^{-1})	k_2 (g mg^{-1} min^{-1})	R^2
CS-Gln-2	25.4	6.5	0.0426	0.433	26.8	0.001392	0.998

Table 3 Isothermal model for uranium adsorption using CS-Gln2

	Freundlich					Sips	
T (K)	K_F	n_f	R^2	q_m (mg g^{-1})	K_s (L mg^{-1})	n_s	R^2
CS-Gln-2	4.63567	1.0425	0.97418	294	0.02719	0.67097	0.97919

Table 4 Comparison of the adsorption performance of CS-Gln with that of other adsorbents

Adsorbent	Conditions	Equilibrium time (min)	q_{max} (mg g^{-1})	Reference
DTAB/TiO_2	pH = 5.0 ± 0.1, T = 298 K	240	108.4	14
COP-CN	pH = 4.5, T = 298 K	15	214	23
DA/C	pH = 7.0, T = 288 K	120	30.4	40
PGC	pH = 5, T = 303 K	120	199.13	41
IPCL	pH = 5, T = 298 K	120	278.8	42
Chitosan/nano-TiO_2	pH = 5.0, T = 298 K	100	259.91	43
MXene-CS	pH = 6, T = 303 K	360	141.96	44
BC@CSPTI	pH = 6, T = 298 K	60	633.4	17
PCAR	pH = 6, T = 308 K	200	561.28	45
CS-Gln2	pH = 6, T = 298 K	2	294	This work

adsorption.[36,38] Based on the fitted curves and experimental parameters, it is evident that all the correlation coefficients (R^2) obtained by fitting with the three models are greater than 0.97. Additionally, the correlation coefficient (R^2) obtained from the Sips isothermal model is slightly greater, which is 0.979. Different types of amino, –COOH and –OH can also cause heterogeneous sorption.[39] Meanwhile, n_f is bigger than 1, and the fitted curve is nonlinear (Table 3 and Fig. 5f), which suggests that the sorption active sites are heterogeneous, and the sorption process involves sorption mechanisms such as surface deposition and hydrogen bonding.[38] Therefore, it can be assumed that there are both monolayer homogeneous adsorption and multi-layer heterogenous adsorption in the uranium adsorption of CS-Gln2. The maximum uranium capture amount is 294 mg g^{-1}, which is calculated by applying the Sips isothermal model with the biggest correlation coefficient (R^2 = 0.979). Herein, the equilibrium contact time and uranium sorption amount of CS-Gln2 are compared with those of other uranium-removing materials (Table 4). The first three are other types of materials, while the others are chitosan-based materials. The mechanism of uranium removal for all the materials mentioned above is adsorption. Compared with the other adsorbents, the sorption amount of CS-Gln2 is not so large, while the equilibrium adsorption time is the shortest.

3.2.4 Influence of actual seawater. It is acknowledged that the overall uranium capacity in seawater is about 4.5 billion tons.[46] If uranium can be extracted from seawater, which will be of great help for the lack of uranium. The static adsorption experiment of CS-Gln for actual seawater is conducted, and the seawater is from Jinting Bay, Shanwei, Guangdong. After 5 days of static adsorption, the adsorption capacity was 4.5 mg g^{-1} for Ca, 97 μg g^{-1} for Zn, and 143 μg g^{-1} for uranium (Fig. 6). There are a large amount of competing ions, such as Fe, Ca, Na and K, which can reduce the uranium adsorption capacity of the material.[47] However, there are many bacterial colonies and sand, which can also reduce uranium adsorption capacity.[48]

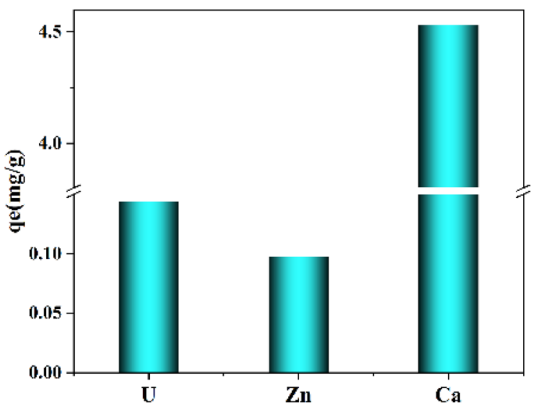

Fig. 6 Selective adsorption of CS-Gln2 in a seawater sample.

3.3 Adsorption mechanism

The surface morphology of CS-Gln2 before and after the capture of U(VI) was detected by applying SEM (Fig. S3), and the elemental analysis of CS-Gln2 after the capture of U(VI) was carried out by applying SEM-EDX (Fig. 7). The surface pores of CS-Gln2 significantly decrease after the capture of U(VI) (Fig. S3). The X-ray spectrum (Fig. 7a) shows distinct uranium peaks from

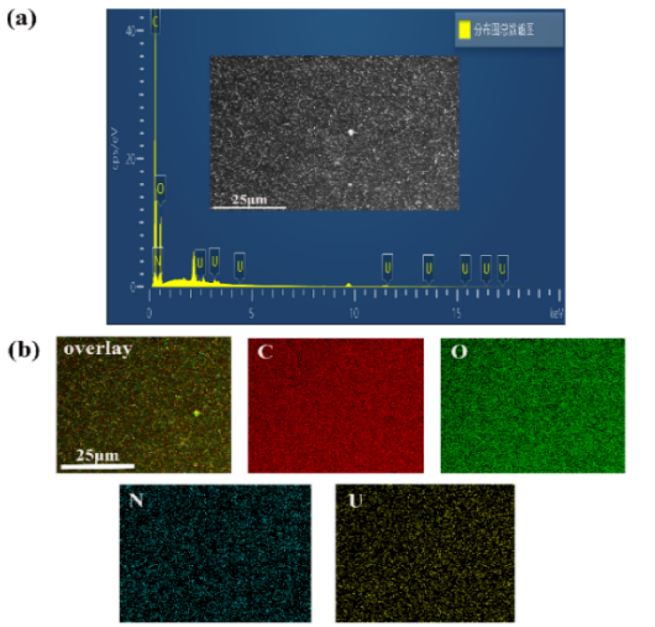

Fig. 7 (a) X-ray diffraction spectrum and (b) EDS mapping of elemental distribution for CS-Gln-U.

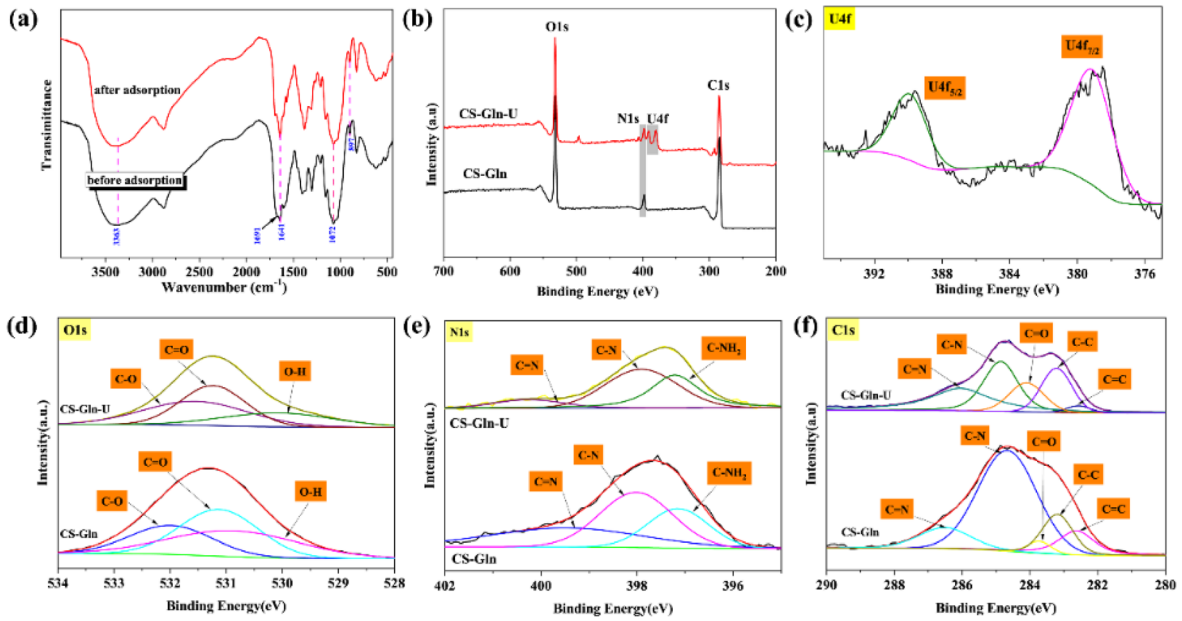

Fig. 8 (a) FT-IR, (b) full XPS, and high-resolution XPS spectra of (c) U 4f, (d) O 1s, (e) N 1s and (f) C 1s of CS-Gln before and after the capture U(VI).

2 eV to 3.5 eV, confirming the successful capture of uranium on CS-Gln. Fig. 7b depicts the uniform distribution of uranium, which correlates with the C/N/O distribution.

The surface functional groups of CS-Gln after the capture of U(VI) were detected by FT-IR (Fig. 8a). After the capture of U(VI), the overlapping peak of $-NH_2$ and OH, originally at 3363 cm^{-1}, is redshifted to 3369 cm^{-1}. Besides, the –COOH peak shifts from 1691 cm^{-1} to 1689 cm^{-1}, while the –C=N peak is blue shifted from 1641 cm^{-1} to 1642 cm^{-1}. The –OH peak at 1072 cm^{-1} is also shifted to 1071 cm^{-1}. As analysed above, all the –COOH, $-NH_2$, –C=N, and –OH groups of CS-Gln are coordinated with uranium.[49] The glycosidic bond at 897 cm^{-1} is moved to 899 cm^{-1} due to overlapping with O=U=O,[50] which further indicates that uranium is successfully enriched after sorption.

After the capture of U(VI), the double peaks at 390 eV and 379 eV belong to U $4f_{5/2}$ and U $4f_{7/2}$ (Fig. 8b and c), respectively, further confirming the successful capture of uranium.[51] For pure CS-Gln2, the high-resolution XPS spectrum of the O 1s can be split into three components (Fig. 8d and Table S2): C–O (531.99 eV), C=O (531.13 eV) and O–H (530.87 eV).[52] After uranium capture, all the peaks of C–O, C=O and O–H shift to 531.54 eV, 531.23 eV and 530.07 eV, respectively. This indicates that both the –COOH and –OH of CS-Gln have a strong coordination capability with U(VI). The N 1s XPS spectrum can be separated into C=N (399.47 eV), C–N (397.15 eV) and C–NH_2 (398.02 eV) (Fig. 8e),[53] respectively. After uranium adsorption, the peak shift of C=N is the biggest, which is redshifted to 400.26 eV. There is little difference in the displacement of C–N and C–NH_2, which are blue-shifted to 397.93 eV and redshifted to 397.21 eV, respectively. This suggests that both C=N and $-NH_2$ also have strong coordination capabilities with U(VI). The C 1s can be deconvoluted into five peaks, that is, 286.51 for C=N, 284.67 eV for C–N, 283.73 eV for C=O, 283.19 eV for C–C and 282.63 for C=C (Fig. 8f).[54] After the uptake of uranium, the most noticeable changes are C=N and C=O, which are shifted at 0.45 eV and 0.36 eV, and the peaks move to 286.06 eV and 284.09 eV, respectively. This result is consistent with the previous analysis and confirms that C=N and –COOH have strong coordination with uranium. To sum up, both electrostatic and coordination effects are involved in uranium sorption by CS-Gln. Among them, –COOH, $-NH_2$, –C=N and –OH are all involved in coordination.

4 Conclusions

A novel and eco-friendly material (CS-Gln) dominated by macropores was successfully prepared by crosslinking chitosan with glutamine. The three-dimensional microporous structure favors uranyl ion diffusion, so the adsorption equilibrium time for uranium by CS-Gln is ultra-fast. The kinetic experiments show that uranium adsorption equilibrium can be reached within 2 min, while complete equilibrium can be reached within 30 min. The adsorption is more consistent with the pseudo-second-order kinetic model and the Sips isothermal model, which are mainly controlled by chemisorption. Additionally, there are both monolayer adsorption and multilayer adsorption for uranium, with the maximum capture amount of 294 mg g^{-1}. The U(VI) sorption of CS-Gln is achieved through the electrostatic attraction on the surface of the adsorbent and the coordination effect of –COOH, $-NH_2$ and –C=N with uranium, and the coordination plays a main role.

Author contributions

Lirong Yang: methodology, investigation, writing – review & editing. Tingdong Zhou: writing – original draft. Yuqian Jiang: data curation. Jie Tang: writing – original draft. Huizhou Chen: data curation. Wenjing Yang: data curation. Haoyu Huang:

visualization. Jianguo Gao: conceptualization, resources, supervision. Deming Huang: conceptualization, supervision.

Conflicts of interest

There are no conflicts to declare.

Data availability

Data will be made available on request.

Supplementary information (SI) is available. See DOI: https://doi.org/10.1039/d5ra04402b.

Acknowledgements

This work was financially supported by the Scientific Research Start-up Project of Mianyang Teachers' College (QD2023A54, QD2018A004), Key Laboratory of materials and surface technology (Ministry of Education), Xihua University (xxx-2024-yb005), Sichuan Province Key Laboratory of Powder Metallurgy, Chengdu University (SC-FMYJ2021-08), Education Department of Sichuan Province (18ZA0252), and Student's Research and Innovation Fund of Sichuan Province (S202410639004, S202410639003).

Notes and references

1 D. Karley, S. K. Shukla and T. S. Rao, *J. Environ. Chem. Eng.*, 2022, **10**(108050).
2 L. Liu, H. Guo, L. Dai, M. Liu, Y. Xiao, T. Cong and H. Gu, *Prog. Nucl. Energy*, 2023, **162**, 104772.
3 T. E. Rehm, *Curr. Opin. Chem. Eng.*, 2023, **39**, 100878.
4 V. A. Sidorenko, *Phys. Atom. Nucl.*, 2013, **76**, 1621–1630.
5 P. Pöml and B. Burakov, *Radiochim. Acta*, 2018, **106**, 985–990.
6 Y. Yokokohji, *Annu. Rev. Control Robot. Auton. Syst.*, 2021, **4**, 681–710.
7 E. J. Bromet, *J. Radiol. Prot.*, 2012, **32**, 71–75.
8 Y. Li, H. Lu, Y. Du, J. Qiu, P. Lin and J. Lin, *Chin. J. Struct. Chem.*, 2025, **44**, 100562.
9 H. Pei, Z. Dong, Z. Li, J. Huang, Y. Jiang, Z. Li, L. Xu, X. Cao, Y. Liu, Z. Zhang and G. Yang, *Nano Res.*, 2024, **17**, 6849–6859.
10 Z. Dong, D. Zeng, Z. Li, J. Chen, Y. Wang, X. Cao, G. Yang, Z. Zhang, Y. Liu and F. Yang, *Chem. Sci.*, 2024, **15**, 19126–19135.
11 J. Lei, H. Liu, L. Zhou, Y. Wang, K. Yu, H. Zhu, B. Wang, M. Zang, J. Zhou, R. He and W. Zhu, *Chem. Eng. J.*, 2023, 471.
12 Z. Liu, T. Ou, M. Su, H. Peng, G. Song, L. Kong and D. Chen, *Chem. Eng. J.*, 2021, **415**, 128858.
13 L. Y. Yuan, L. Zhu, C. L. Xiao, Q. Y. Wu, N. Zhang, J. P. Yu, Z. F. Chai and W. Q. Shi, *ACS Appl. Mater. Interfaces*, 2017, **9**, 3774–3784.
14 J. Wang, R. Ma and Z. Jiang, *Environ. Sci. Pollut. Res.*, 2022, **30**, 30548–30556.
15 C.-Q. Ruan, M. Strømme and J. Lindh, *Carbohydr. Polym.*, 2018, **181**, 200–207.
16 Y. Liu, Y. Liu, X. Cao, R. Hua, Y. Wang, C. Pang, M. Hua and X. Li, *J. Radioanal. Nucl. Chem.*, 2011, **290**, 231–239.
17 Y. Zhang, B. Mei, B. Shen, L. Jia, J. Liao and W. Zhu, *Carbohydr. Polym.*, 2023, 312.
18 Q. Ren, H. Xia, J. Lv, Y. Wang, C. Yin, Y. Liu, Z. Chen, Y. Li and Y. Wang, *Colloids Surf., A*, 2024, **683**, 133036.
19 Y. Wang, X. Du, Z. Liu, S. Shi and H. Lv, *J. Mater.*, 2019, **7**, 5111–5152.
20 M. P. Chavhan, M. Musielak and V. Slovák, *Microporous Mesoporous Mater.*, 2024, 366.
21 J. Yang, Y. Li, T. Tian, H. Shi, Z. Ahmad, N. Geng, J. Jin, Y. Huang, H. Zhang, H. Fan and J. Chen, *Chem. Eng. J.*, 2023, 465.
22 X. Yang, J. Li, J. Liu, Y. Tian, B. Li, K. Cao, S. Liu, M. Hou, S. Li and L. Ma, *J. Mater. Chem. A*, 2014, **2**, 1550–1559.
23 X. Li, Y. Zou, Z. Jia, J. Zhang, Y. Li, X. Guo, M. Zhang, K. Li, J. Li and L. Ma, *J. Hazard. Mater.*, 2021, **401**(123802).
24 S. R. Mukai, *J. Jpn. Pet. Inst.*, 2011, **54**(3), 127–135.
25 V. Linsha, A. Peer Mohamed and S. Ananthakumar, *Chem. Eng. J.*, 2015, **259**, 313–322.
26 S. R. Mukai, *J. Jpn. Pet. Inst.*, 2011, **54**(3), 127–135.
27 Y. Xiao, B. Hu, Y. Guo, D. Zhang, Y. Zhao, Y. Chen, N. Li and L. Yu, *Curr. Treat. Options Oncol.*, 2023, **24**, 1021–1035.
28 S. M. Rafigh and A. Heydarinasab, *ACS Sustain. Chem. Eng.*, 2017, **5**, 10379–10386.
29 M. Kasaai, *Carbohydr. Polym.*, 2008, **71**, 497–508.
30 B. Chen, H. Zhao, S. Chen, F. Long, B. Huang, B. Yang and X. Pan, *Chem. Eng. J.*, 2019, **356**, 69–80.
31 K. K. A. a. J. B. Krishnankutty-Nair and P. Kumar, *J. Mater. Chem. A*, 1993, **3**, 1141–1149.
32 M. Kaur, P. Tewatia, G. Rattan, S. Singhal and A. Kaushik, *J. Hazard. Mater.*, 2021, **417**, 126060.
33 Y. Liu, Z. Shi, Y. Gao, W. An, Z. Cao and J. Liu, *ACS Appl. Mater. Interfaces*, 2016, **8**, 28283–28290.
34 J. Liu, D. Ma, X. Zhang, L. Li, L. Liu, Y. Gao and Z. Cao, *Ionics*, 2023, **29**, 1173–1185.
35 L. Yang, F. Chen, D. Chen, J. Gao, H. Ju, J. Tang, Q. Jiang and X. Wang, *J. Environ.*, 2024, **12**, 111955.
36 A. Flilissa, S. Venkataraman, K. Laouameur, A. Beroual, O. Flilissa, K. Omine, T. Chaabane and A. Darchen, *J. Environ.*, 2020, **8**, 103625.
37 H. Zhao, P. Li, F. Su, X. He and V. Elumalai, *Chemosphere*, 2022, 301.
38 X.-D. Xue, C.-R. Fang and H.-F. Zhuang, *J. Hazard. Mater.*, 2021, **407**, 124835.
39 Z. Huang, Z. Li, Q. Wu, L. Zheng, L. Zhou, Z. Chai, X. Wang and W. Shi, *Environ. Sci.: Nano*, 2018, **5**, 2077–2087.
40 W. Zhang, Y. Chen and W. Wu, *J. Mol. Liq.*, 2024, 395.
41 F. Wu, H. Huang, X. Sun, S. Xie, H. Yuan, Y. Liu and Y. Guo, *J. Radioanal. Nucl. Chem.*, 2023, **332**, 3617–3633.
42 H. Wang, L. Zhou, X. Ao, G. Huang, Y. Liu, J. Ouyang and A. A. Adesina, *Int. J. Biol. Macromol.*, 2024, **266**(131113).
43 X. Ao, L. Zhou, J. Jin, Y. Liu, J. Ouyang, Z. Liu and H. Shehzad, *Int. J. Biol. Macromol.*, 2023, **253**, 126966.
44 S. Li, J. He, Y. Wang, J. Qiao, Y. Yang and G. Wang, *Colloids Surf., A*, 2023, 674.
45 X. Zhang, L. Zhang, Q. Wang, Q. Xin, Y. Xiong and H. Wang, *Int. J. Biol. Macromol.*, 2023, **253**, 126661.

46 A. Zhang, T. Asakura and G. Uchiyama, *React. Funct. Polym.*, 2003, **57**, 67–76.
47 G. Tan, X. Xue, Z. Zhu and J. Li, *ACS ES&T Water*, 2021, **1**, 1577–1586.
48 Y. Yuan, Q. Yu, S. Yang, J. Wen, Z. Guo, X. Wang and N. Wang, *Adv. Sci.*, 2019, **6**, 1900961.
49 Q. L. Daikun Li, N. Bai, H. Dong and D. Mao, *ACS Sustain. Chem. Eng.*, 2017, **5**(6), 5598–5607.
50 S. Li, P. Yang, X. Liu, J. Zhang, W. Xie, C. Wang, C. Liu and Z. Guo, *J. Mater.*, 2019, **7**, 16902–16911.
51 L. Yang, Y. Li, D. Chen, J. Gao, S. Shu, X. Pu, H. Yang and J. Tang, *J. Water Proc. Eng.*, 2024, **61**, 105197.
52 T. P. Gandhi, M. S. V. N. Jyothi, S. Gomosta, A. Pamarthi, S. Manna and S. M. Maliyekkal, *J. Clean. Prod.*, 2024, **435**, 140433.
53 M. Zhou, S. Wang, F. Liu and B. Hu, *Sep. Purif. Technol.*, 2024, **338**, 126501.
54 T. P. Gandhi, M. S. V. Naga Jyothi, S. Gomosta, A. Pamarthi, S. Manna and S. M. Maliyekkal, *J. Cleaner Prod.*, 2024, **435**, 140433.